*Domagoj Kojundžić* ✉
*Nikša Krnić*
*Zoran Kožuh*

https://doi.org/10.21278/TOF.481054823
ISSN 1333-1124
eISSN 1849-1391

# INFLUENCE OF ARGON AND HELIUM PURGING FLOW RATES ON THE FUSION ZONE IN AUTOGENOUS STATIONARY TIG ARC WELDING OF 316L STAINLESS STEEL

**Summary**

The impact of argon and helium purging flow rates of 4 l/min and 10 l/min on fusion zone dimensions and shape was investigated. Experiments were performed during an autogenous stationary TIG welding process for welding times of 7 s, 14 s, and 21 s. For a welding time of 7 s, the flow rate of the argon and helium purging gases almost did not affect the fusion zone. When the welding time was extended (14 s), the argon purging flow rate also had no significant effect on the fusion zone. However, increasing the helium purging flow rate resulted in a significant (approx. 20 %) increase in weld penetration. Arc time of 21 s and an argon flow rate of 10 l/min decreased the weld penetration by around 17 %. On the other hand, an increased helium flow rate had the opposite effect, leading to an increase of approx. 17 % in weld penetration.

*Key words:* *purging gas flow rate; argon; helium; fusion zone dimensions; stationary TIG welding; 316L stainless steel*

## 1. Introduction

The austenitic stainless steel (ASS) alloys are a subset of the wide stainless steel family. These alloys are based on iron and contain significant amounts of chromium and nickel. Compared to carbon steels, ASS alloys have significantly lower thermal and electrical conductivity, while their thermal expansion is substantially higher. They are widely used in the chemical, food, transportation, and oil industries because of their corrosion and oxidation resistance. ASS alloys also have relatively good formability and weldability [1], [2].

A lot of effort has been put into research on the weldability of ASS alloys. Consequently, most of the welding processes have been applied to join these alloys. One of the most commonly used welding processes for joining ASS alloys is Tungsten Inert Gas (TIG) welding or Gas Tungsten Arc (GTA) welding. This process is characterised by its versatility and high joint quality, but it has relatively low productivity and shallow fusion zone depth (weld penetration) [3]. The TIG fusion zone width (W) is usually significantly larger compared to its depth (D), which results in a low depth-to-width (D/W) ratio, also known as the weld aspect ratio. The formation of the fusion zone under the electric arc and its evolution are highly complex

processes controlled by heat transfer dynamics. The shape of the weld joint is a key characteristic that significantly affects the performance and structural integrity of the welding process [4], [5], [6]. Several different forces inside the arc and weld pool regions act simultaneously and affect energy transfer, thus determining the final fusion zone shape. The TIG welding parameters control the amount of heat generated in the arc, along with the intensity and direction of the forces inside the arc [7], [8], [9]. Many researchers have investigated the TIG fusion zone because of its importance and complex evolution. Fusion zone geometry is usually described by its width and depth, or a simple D/W ratio. Several research studies dealing with autogenous TIG fusion zone shape and its correlation with welding parameters were carried out on various ASS alloy base metals (304, 316, 316L) [10], [11], [12], [13], [14]. It is important to point out that these studies indicate that very small variations in the amount (parts per million, or ppm) of surface-active elements (elements such as S, O, and Se) in stainless steel can result in significantly different shapes and dimensions of fusion zones formed under the same conditions (welding parameters) [9], [15], [16]. This is because surface-active elements change the liquid metal surface tension, which is one of the dominant convection-governing forces. Convectiev heat transfer is especially important in stainless steel weld pool formation because of the low thermal conductivity of stainless steel alloys [7], [17].

The welding of stainless steels requires the use of root-side shielding gas, often called purging or backing gas, which prevents oxidation on the weld root side. This ensures the formation of a high-quality welded joint that retains its corrosion resistance [2]. The most commonly used purging gases are helium, argon, nitrogen, and their mixtures with hydrogen. In the available scientific literature, the authors investigated the effect of purging gas on the strength, corrosion resistance, and microstructure of the welded joint [18], [19], [20], [21].

Compared to the mobile TIG welding , significantly less research has been done on the stationary (spot) welding. Stadler et al. [22] [23] investigated the effects of welding current, arc length, shielding gas type, and tungsten electrode vertex angle on the 304L base metal. The influence of the chemical composition of root-side purging gas on the fusion zone geometry in stationary TIG welding was studied in [24]. The authors showed that argon purging increased the penetration depth and cross-section area compared to helium purging.

However, no previous study has investigated the effect of purging gas flow rate on the fusion zone geometry in stationary TIG welding. This study was designed to investigate the effect of argon and helium purging gas flow rates on the dimensions of the characteristic fusion zone. The chosen flow rates were 4 and 10 l/min. Stationary TIG welding experiments were conducted on the 316L austenitic stainless steel for welding times of 7 s, 14 s, and 21 s.

## 2. Experimental work and methodology

### 2.1 Experimental setup

The laboratory setup enabled time-controlled stationary autogenous TIG welding. The welding power source (the INVERTER ACCUTIG AVP-300P) was controlled by a self-developed system based on an Arduino microcontroller. The system reacts to the light signal from the electric arc and enables a 0.1-second timing resolution of welding time. The light from the electric arc was captured by an optical fibre cable at the welding start and then transmitted to the light-dependent resistor (LDR) that was connected to the Arduino microcontroller. At the moment when the timer counted down the selected welding time, the power supply was switched off and the electric arc was extinguished. The welding power source can be used for AC, DC, or pulsed TIG welding with a current intensity of up to 300 A. The welding gun was air-cooled and equipped with a collet for a 2.4 mm electrode. A 2 % thorium oxide-doped tungsten electrode (Ø 2.4 mm) with a cone-shaped 45° vertex without truncation was used. The electrode tip was longitudinally sharpened on a tungsten electrode grinder according to accepted practice.

The self-developed four-point symmetric fixture for specimen positioning was used to minimise thermal contact heat losses from the specimen, prevent arc blow, and enable symmetric current flow through the base metal. Thus, specimens were cooled during and after the TIG welding, primarily by natural convection and radiation heat transfer. The second fixture was used to position the welding gun (tungsten electrode) at the desired location above the specimen during the welding experiment. It had three axes of freedom, which enabled the placement of the tungsten electrode in the vertical position above the specimen centre and electric arc length adjustment.

The system for the purging gas application ensured a uniform gas supply on the specimen's bottom (root) side. It consists of a flow regulator, supply pipes, and a square steel tube (45 mm x 45 mm) positioned 1 mm from the specimen. Perforated sheet metal was inserted into the pipe to distribute the purging gas flow evenly. The schematic representation and a photo of the described experimental setup are shown in Fig. 1.

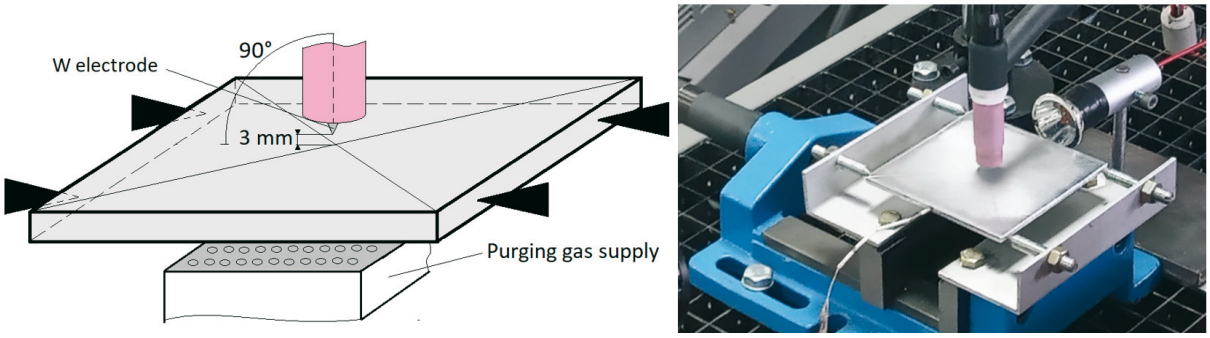


**Fig. 1** Experimental welding setup

## 2.2 Base metal and purging gases

Specimens used in this research were 5 mm thick and 100 x100 mm square-shaped. They were cut from a strip of AISI 316L (EN 1.4404 X2CrNiMo17-12-2) austenitic stainless steel. The AISI 316L steel type is a highly alloyed low-carbon stainless steel suitable for welding and different structural applications requiring resistance to pitting corrosion. This steel was subjected to the 1D mill finish after hot rolling, annealing (at 1050 °C), and scale removal (pickling) according to the manufacturer. The chemical composition of AISI 316L stainless steel is presented in Table 1. Solidus and liquidus temperatures for 316L ASS are 1402 °C and 1435 °C, respectively [25].

**Table 1** The chemical composition of AISI 316L stainless steel

| El. | C | Si | Mn | P | S | Cr | Ni | Mo | N |
|---|---|---|---|---|---|---|---|---|---|
| wt. / % | 0.023 | 0.571 | 1.36 | 0.0289 | 0.0111 | 17.067 | 10.558 | 2.14 | 0.0556 |

The role of gas purging on the weld root side is to prevent the formation of thicker surface oxides on stainless steel, thus enabling the formation of high-quality joints and reducing the potential for pitting and intergranular corrosion. Common purging gases include argon, nitrogen, helium, and their mixtures with hydrogen. In this research, argon (4.8 purity grade) and helium (5.0 purity grade) were chosen as purging gases, and argon was also used as a shielding gas in all experiments. The aim was to investigate the effect of the flow rates of both gases on the stationary TIG fusion zone.

Helium and argon differ significantly regarding their thermal and physical properties. Helium is significantly lighter than air, with about 14% of the air density. On the other hand, argon is 1.38 times heavier than air. The thermal conductivities of argon and helium are shown in Fig. 2.

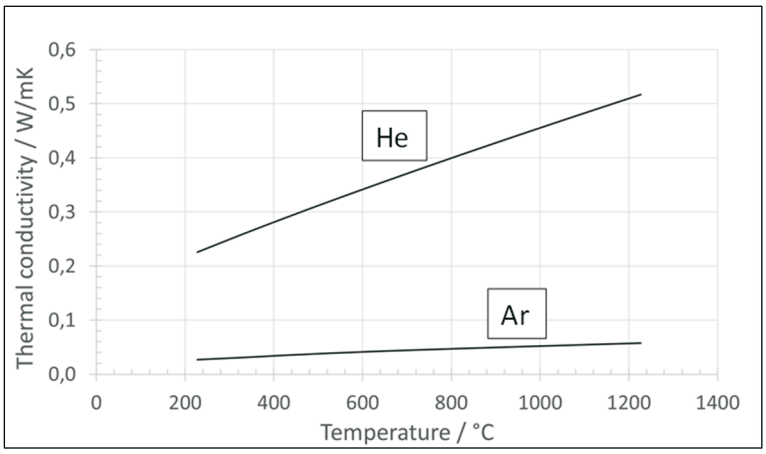


**Fig. 2** The thermal conductivities of helium and argon used as purging gases according to the data from [26]

## 2.3 Plan of the experiments

The focus of this research was to examine the effects of the purging gas flow rate on the stationary autogenous TIG fusion zone dimensions. Experiments were performed under the same welding conditions on 5 mm-thick 316L stainless steel base metal. A minimum of three repetitions of the experiment for every observed welding time were performed. Some experiments were repeated more than three times if fusion zone depth values diverged significantly. The experimental design is summarised in **Table 2**. The measured characteristic fusion zone dimensions enabled the calculations of mean values and assured an insight into the process repeatability.

**Table 2** Experimental design

| Experimental category | Welding time | Shielding gas, and its flow rate |
|---|---|---|
| Ar4_7s | 7 s | Argon, 4 l/min |
| Ar10_7s | 7 s | Argon, 10 l/min |
| Ar4_14s | 14 s | Argon, 4 l/min |
| Ar10_14s | 14 s | Argon, 10 l/min |
| Ar4_21s | 21 s | Argon, 4 l/min |
| Ar10_21s | 21 s | Argon, 10 l/min |
| He4_7s | 7 s | Helium, 4 l/min |
| He10_7s | 7 s | Helium, 10 l/min |
| He4_14s | 14 s | Helium, 4 l/min |
| He10_14s | 14 s | Helium, 10 l/min |
| He4_21s | 21 s | Helium, 4 l/min |
| He10_21s | 21 s | Helium, 10 l/min |

## 2.4 Welding procedure

Hand grinding was performed on all specimens to ensure uniform surface roughness and eliminate any irregularities from the manufacturing process. The top side of each specimen was ground using silicon carbide sandpaper of three different grain sizes, i.e., first P#120, then P#400, and finally P#800. The root side of the specimen was initially ground using an electrically-driven hand grinding machine. Subsequently, the same hand grinding procedure as that on the top side was used. A portable SJ301 surface roughness tester was used to measure the obtained surface roughness. Average $R_a$ values of 1.81 and 1.14 were determined for the face and the root side, respectively. Before the welding experiment, every specimen was

thoroughly degreased using denatured alcohol. The positioning of the specimen required special care to ensure an accurate horizontal position in the fixture because even small inaccuracies can result in an asymmetric fusion zone shape.

Purging gas flow rates of 10 l/min for argon and 4 l/min for helium were initially chosen as minimum gas flow rates that still provide quality root side shielding for a welding time of 21 s. Then, it was decided to investigate whether changing the gas flow rates had any effect on the resulting fusion zone dimensions. Thus, the flow rate of helium was increased from 4 l/min to 10 l/min. The flow rate meter was calibrated for argon gas.

The same welding parameters, summarised in **Table 3**, were used in all welding experiments. The weld root side purging gas type (argon or helium), the corresponding flow rate (4 or 10 l/min), and welding time (7, 14, and 21 s) were varied according to the plan of the experiment. This procedure enabled us to determine the relationship between the purging gas flow rate (argon and helium) and the characteristic fusion zone dimensions.

**Table 3** Welding parameters

| **Welding parameter** | |
|---|---|
| Current type | Direct current (DC) |
| Electrode polarity | Electrode negative (EN, SP) |
| Current intensity | 150 A |
| W electrode diameter | 2.4 mm |
| W electrode type | 2% Th (red labelled) |
| Vertex angle of the W electrode | 45° |
| Truncation of the W electrode | 0 mm |
| W electrode stick-out | 3 mm |
| Gap from W electrode tip to BM | 3 mm |
| Electrode-to-workpiece angle | 90° |
| Shielding gas | Argon 4.8 |
| Shielding gas flow rate | 8 l/min |
| Shielding gas nozzle diameter | Ø 11 mm (size 7) |
| Welding position | PA (downhand, flat) |

## 2.5 Metallographic analysis

The metallographic analysis was carried out to reveal the weld fusion line and evaluate the resulting fusion zone dimensions. A metallography sectioning saw with water cooling was used to cut the specimens precisely along the fusion zone diameter, thus allowing an insight into the weld cross-section. To prepare the specimen cross-section for etching, it was ground in three steps, ending with waterproof silicon carbide sandpaper (P#180 grain size, according to the FEPA standard). The etching was performed in a mixture of water, hydrofluoric, and hydrochloric acids (in the ratio of 5:4:2). After etching, the weld-bead zone macrostructure was finally revealed. The cross-section was then photographed using a stereo-zoom optical microscope under the appropriate magnification.

The fusion zone photo was then analysed using the open-source ImageJ image processing software. The fusion zone width, depth, and cross-section area were measured because they are considered to be convenient fusion zone characteristics. The measurements were calibrated using the thickness of the specimen. If the maximum fusion zone depth was not located in the middle, the maximum lateral penetrations and the middle penetration were averaged, and that value was regarded as penetration. The fusion zone depth-to-width ratio (D/W ratio) was also calculated because of its wide acceptance. The measurement error caused by random factors was in a range of approximately ±2%.

## 3. Results

The measured fusion zone (FZ) width, depth, and cross-section area for argon and helium flow rates of 4 and 10 l/min are presented in Tables 4–7. If the experiment resulted in a full penetration of 5 mm, the width of the fusion zone on the root side was also measured. The tables contain data for welding times of 7, 14, and 21 s.

**Table 4** Fusion zone dimensions for the argon flow rate of 4 l/min

| *Welding time:* 7 s | | | | | *Welding time:* 14 s | | | | | *Welding time:* 21 s | | | | |
|---|---|---|---|---|---|---|---|---|---|---|---|---|---|---|
| *Exp. cat.* | *Width* mm | *Depth* mm | *Area* mm$^2$ | *Root dia.* mm | *Exp. cat.* | *Width* mm | *Depth* mm | *Area* mm$^2$ | *Root dia.* mm | *Exp. cat.* | *Width* mm | *Depth* mm | *Area* mm$^2$ | *Root dia.* mm |
| ***Ar4_7s*** | 11.90 | 1.48 | 15.26 | 0.00 | ***Ar4_14s*** | 14.40 | 2.25 | 30.44 | 0.00 | ***Ar4_21s*** | 15.90 | 3.44 | 47.00 | 0.00 |
| ***Ar4_7s*** | 11.15 | 1.52 | 16.49 | 0.00 | ***Ar4_14s*** | 13.70 | 2.65 | 34.14 | 0.00 | ***Ar4_21s*** | 14.80 | 5.00 | 69.62 | 11.20 |
| ***Ar4_7s*** | 11.20 | 1.69 | 16.90 | 0.00 | ***Ar4_14s*** | 13.75 | 2.61 | 33.63 | 0.00 | ***Ar4_21s*** | 14.40 | 5.00 | 74.95 | 11.80 |
| ***St. de.*** | 0.42 | 0.11 | 0.85 | 0.00 | ***St. de.*** | 0.39 | 0.22 | 2.01 | 0.00 | ***St. de.*** | 0.78 | 0.90 | 14.84 | 6.65 |

**Table 5** Fusion zone dimensions for the argon flow rate of 10 l/min

| *Welding time* 7 s | | | | | *Welding time* 14 s | | | | | *Welding time* 21 s | | | | |
|---|---|---|---|---|---|---|---|---|---|---|---|---|---|---|
| *Exp. cat.* | *Width* mm | *Depth* mm | *Area* mm$^2$ | *Root dia.* mm | *Exp. cat.* | *Width* mm | *Depth* mm | *Area* mm$^2$ | *Root dia.* mm | *Exp. cat.* | *Width* mm | *Depth* mm | *Area* mm$^2$ | *Root dia.* mm |
| ***Ar10_7s*** | 11.70 | 1.59 | 16.10 | 0.00 | ***Ar10_14s*** | 13.75 | 3.59 | 43.00 | 0.00 | ***Ar10_21s*** | 15.43 | 4.22 | 54.36 | 0.00 |
| ***Ar10_7s*** | 11.85 | 1.42 | 14.70 | 0.00 | ***Ar10_14s*** | 13.90 | 2.89 | 35.35 | 0.00 | ***Ar10_21s*** | 16.20 | 3.55 | 45.68 | 0.00 |
| ***Ar10_7s*** | 11.80 | 1.38 | 15.21 | 0.00 | ***Ar10_14s*** | 14.05 | 2.50 | 34.83 | 0.00 | ***Ar10_21s*** | 15.70 | 3.93 | 52.20 | 0.00 |
| ***St. de.*** | 0.08 | 0.11 | 0.71 | 0.00 | ***St. de.*** | 0.15 | 0.55 | 4.57 | 0.00 | ***St. de.*** | 0.39 | 0.34 | 4.52 | 0.00 |

**Table 6** Fusion zone dimensions for the helium flow rate of 4 l/min

| *Welding time* 7 s | | | | | *Welding time* 14 s | | | | | *Welding time* 21 s | | | | |
|---|---|---|---|---|---|---|---|---|---|---|---|---|---|---|
| *Exp. cat.* | *Width* mm | *Depth* mm | *Area* mm$^2$ | *Root dia.* mm | *Exp. cat.* | *Width* mm | *Depth* mm | *Area* mm$^2$ | *Root dia.* mm | *Exp. cat.* | *Width* mm | *Depth* mm | *Area* mm$^2$ | *Root dia.* mm |
| ***He4_7s*** | 11.80 | 1.48 | 15.80 | 0.00 | ***He4_14s*** | 13.90 | 2.50 | 32.84 | 0.00 | ***He4_21s*** | 15.90 | 3.35 | 43.82 | 0.00 |
| ***He4_7s*** | 11.50 | 1.45 | 15.51 | 0.00 | ***He4_14s*** | 13.80 | 2.78 | 36.20 | 0.00 | ***He4_21s*** | 15.85 | 3.42 | 46.54 | 0.00 |
| ***He4_7s*** | 11.55 | 1.42 | 15.40 | 0.00 | ***He4_14s*** | 13.80 | 2.46 | 31.10 | 0.00 | ***He4_21s*** | 16.25 | 2.88 | 40.83 | 0.00 |
| ***St. de.*** | 0.16 | 0.03 | 0.21 | 0.00 | ***St. de.*** | 0.06 | 0.17 | 2.59 | 0.00 | ***St. de.*** | 0.22 | 0.29 | 2.86 | 0.00 |

**Table 7** Fusion zone dimensions for the helium flow rate of 10 l/min

| *Welding time* 7 s | | | | | *Welding time* 14 s | | | | | *Welding time* 21 s | | | | |
|---|---|---|---|---|---|---|---|---|---|---|---|---|---|---|
| *Exp. cat.* | *Width* mm | *Depth* mm | *Area* mm$^2$ | *Root dia.* mm | *Exp. cat.* | *Width* mm | *Depth* mm | *Area* mm$^2$ | *Root dia.* mm | *Exp. cat.* | *Width* mm | *Depth* mm | *Area* mm$^2$ | *Root dia.* mm |
| ***He10_7s*** | 11.35 | 1.48 | 16.10 | 0.00 | ***He10_14s*** | 13.95 | 2.31 | 29.90 | 0.00 | ***He10_21s*** | 15.50 | 3.52 | 48.60 | 0.00 |
| ***He10_7s*** | 10.70 | 2.58 | 24.70 | 0.00 | ***He10_14s*** | 13.20 | 4.66 | 47.49 | 0.00 | ***He10_21s*** | 15.50 | 3.84 | 51.69 | 0.00 |
| ***He10_7s*** | 11.30 | 1.59 | 17.01 | 0.00 | ***He10_14s*** | 13.15 | 3.36 | 38.34 | 0.00 | ***He10_21s*** | 14.75 | 5.00 | 73.20 | 11.03 |
| ***St. de.*** | 0.36 | 0.61 | 4.72 | 0.00 | ***St. de.*** | 0.45 | 1.18 | 8.80 | 0.00 | ***St. de.*** | 0.43 | 0.78 | 13.30 | 6.37 |

If a larger standard deviation was observed in the depth of penetration, additional experiments were performed. Their results are shown in Tables 8-11.

**Table 8** Results of additional experiments for the argon flow rate of 4 l/min

| *Welding time* 7 s | | | | | *Welding time* 14 s | | | | | *Welding time* 21 s | | | | |
|---|---|---|---|---|---|---|---|---|---|---|---|---|---|---|
| *Exp. cat.* | *Width* mm | *Depth* mm | *Area* mm$^2$ | *Root dia.* mm | *Exp. cat.* | *Width* mm | *Depth* mm | *Area* mm$^2$ | *Root dia.* mm | *Exp. cat.* | *Width* mm | *Depth* mm | *Area* mm$^2$ | *Root dia.* mm |
| ***Ar4_7s*** | | | | | ***Ar4_14s*** | 13.15 | 5.00 | 53.75 | 0.00 | ***Ar4_21s*** | 14.85 | 5.00 | 74.68 | 11.95 |
| ***Ar4_7s*** | | | | | ***Ar4_14s*** | 13.70 | 3.78 | 41.40 | 0.00 | ***Ar4_21s*** | 15.10 | 5.00 | 74.29 | 10.35 |
| ***Ar4_7s*** | | | | | ***Ar4_14s*** | 14.40 | 2.65 | 30.55 | 0.00 | ***Ar4_21s*** | 15.80 | 4.10 | 52.53 | 0.00 |

**Table 9** Results of additional experiments for the argon flow rate of 10 l/min

| *Welding time* 7 s | | | | | *Welding time* 14 s | | | | | *Welding time* 21 s | | | | |
|---|---|---|---|---|---|---|---|---|---|---|---|---|---|---|
| *Exp. cat.* | *Width* mm | *Depth* mm | *Area* mm$^2$ | *Root dia.* mm | *Exp. cat.* | *Width* mm | *Depth* mm | *Area* mm$^2$ | *Root dia.* mm | *Exp. cat.* | *Width* mm | *Depth* mm | *Area* mm$^2$ | *Root dia.* mm |
| ***Ar10_7s*** | | | | | ***Ar10_14s*** | 13.75 | 3.07 | 37.81 | 0.00 | ***Ar10_21s*** | 16.00 | 3.72 | 49.16 | 0.00 |
| ***Ar10_7s*** | | | | | ***Ar10_14s*** | 13.60 | 3.26 | 40.14 | 0.00 | ***Ar10_21s*** | 15.75 | 3.53 | 46.44 | 0.00 |

**Table 10** Results of additional experiments for the helium flow rate of 4 l/min

| *Welding time* 7 s | | | | | *Welding time* 14 s | | | | | *Welding time* 21 s | | | | |
|---|---|---|---|---|---|---|---|---|---|---|---|---|---|---|
| *Exp. cat.* | *Width* mm | *Depth* mm | *Area* mm$^2$ | *Root dia.* mm | *Exp. cat.* | *Width* mm | *Depth* mm | *Area* mm$^2$ | *Root dia.* mm | *Exp. cat.* | *Width* mm | *Depth* mm | *Area* mm$^2$ | *Root dia.* mm |
| ***He4_7s*** | | | | | ***He4_14s*** | 14.00 | 2.48 | 32.53 | 0.00 | ***He4_21s*** | 15.70 | 3.64 | 46.48 | 0.00 |
| ***He4_7s*** | | | | | ***He4_14s*** | 13.40 | 3.00 | 37.43 | 0.00 | ***He4_21s*** | 15.30 | 5.00 | 71.68 | 8.95 |
| ***He4_7s*** | | | | | ***He4_14s*** | | | | | ***He4_21s*** | 15.60 | 3.69 | 48.90 | 0.00 |

**Table 11** Results of additional experiments for the helium flow rate of 10 l/min

| *Welding time* 7 s | | | | | *Welding time* 14 s | | | | | *Welding time* 21 s | | | | |
|---|---|---|---|---|---|---|---|---|---|---|---|---|---|---|
| *Exp. cat.* | *Width* mm | *Depth* mm | *Area* mm$^2$ | *Root dia.* mm | *Exp. cat.* | *Width* mm | *Depth* mm | *Area* mm$^2$ | *Root dia.* mm | *Exp. cat.* | *Width* mm | *Depth* mm | *Area* mm$^2$ | *Root dia.* mm |
| ***He10_7s*** | 11.30 | 1.44 | 15.57 | 0.00 | ***He10_14s*** | 13.50 | 2.75 | 34.44 | 0.00 | ***He10_21s*** | 15.50 | 4.49 | 53.95 | 0.00 |
| ***He10_7s*** | | | | | ***He10_14s*** | 13.40 | 3.56 | 42.82 | 0.00 | ***He10_21s*** | 15.25 | 4.53 | 53.43 | 0.00 |
| ***He10_7s*** | | | | | ***He10_14s*** | 14.00 | 2.40 | 32.20 | 0.00 | ***He10_21s*** | | | | |

## 4. Discussion

### 4.1 Welding time; 7 s; argon purging

Fig. **3** shows the measured values of the fusion zone width and the corresponding mean values for a welding time of 7 s, with two different argon flow rates on the root side of the weld formed by stationary TIG welding. The reproducibility of the TIG process with regard to the measured widths of the fusion zone was very good: the standard deviation in the measurements for argon flow rates of 4 l/min and 10 l/min was 0.42 and 0.11, respectively. The results show that there is no significant difference between the average width of the fusion zones created under the same welding conditions (parameters) with different argon flow rates on the root side. Namely, by increasing the argon flow rate from 4 l/min to 10 l/min, the average width of the fusion zone increased by only 3.2%. From the facts stated above, one can conclude that the specified change in the flow rate did not have a significant impact on the width of the fusion zone during the welding time of 7 s.

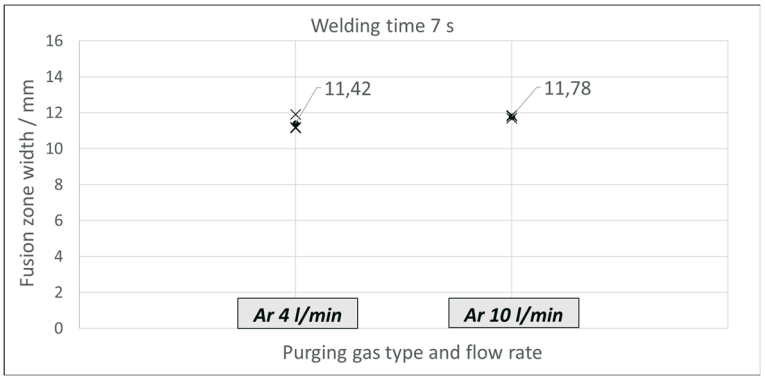


**Fig. 3** Fusion zone widths for two different argon flow rates on the weld root side

The measured depths of the fusion zone and the corresponding mean values for a welding time of 7 s with the argon flow rates on the weld root side of 4 l/min and 10 l/min are shown in Fig. 4. The standard deviation of measured values was 0.11 for both flow rates, i.e., 4 l/min and 10 l/min. This indicates a good reproducibility of the process considering the depth of penetration. The average penetration was 1.56 mm for the argon flow rate of 4 l/min and 1.46 mm for the argon flow of 10 l/min. The difference between the two values of the average penetration amounts to 6.4%, from which it follows that the analysed change in the argon flow rate on the weld root side did not have a strong influence on the depth of the fusion zone during the welding time of 7 s.

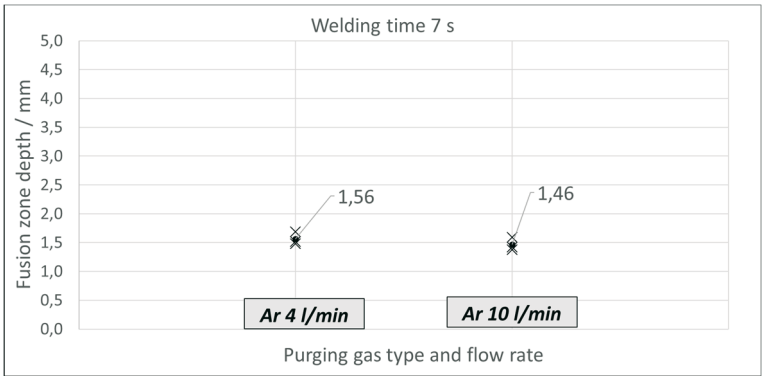


**Fig. 4** Fusion zone depths for two different argon flow rates on the weld root side

Figure 5 shows the characteristic D/W ratios for the fusion zones formed during the welding process (welding time of 7 s and two different argon flow rates, 4 and 10 l/min, on the weld root side). The values correspond to the typical penetration profile of the conventional TIG process, where the width of the fusion zone is significantly greater than its depth. The average fusion zone D/W ratio decreased by 9.5 % when the argon flow rate was increased to 10 l/min.

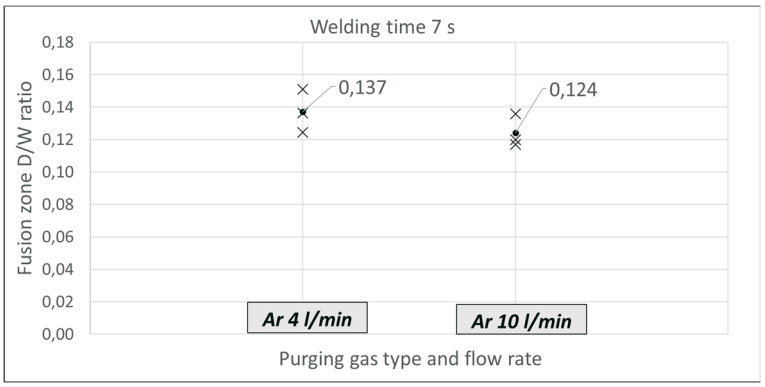


**Fig. 5** Fusion zone D/W ratio for two different argon flow rates on the weld root side

Fig. **6** shows the measured fusion zone cross-section areas for the argon flow rates of 4 and 10 l/min on the weld root side and the welding time of 7 s. The results indicate that changes in the argon flow rates did not significantly affect the fusion zone cross-section area. Increasing the argon flow rate from 4 l/min to 10 l/min resulted in a decrease in the average cross-section of 5.4%.

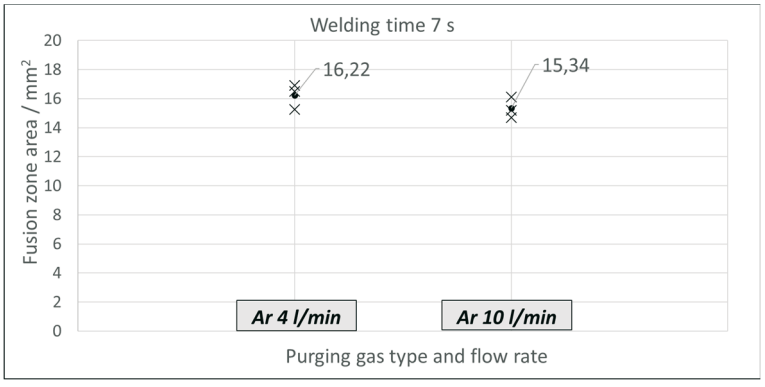


**Fig. 6** Fusion zone area for two different argon flow rates on the weld root side

It can be stated that no significant influence of the argon purging flow rate on the fusion zone dimensions was recorded for the stationary TIG process and welding time of 7 s.

## 4.2 Welding time 7 s; helium purging

The measured values of the fusion zone width and their mean values for a welding time of 7 s and two different helium flow rates on the weld root side are shown in Fig. 7. The narrow intervals in which the measured values were found indicate good reproducibility of the TIG process considering the fusion zone width. For the helium flows of 4 and 10 l/min, the standard deviation in measurements was 0.16 and 0.31, respectively. The measurements show that there is no significant difference between the average width of the fusion zones formed at different helium flow rates on the root side of the weld. By increasing the helium flow rate from 4 l/min to 10 l/min, the average width of the fusion zone decreased by 2.6%. From this, it follows that the analysed change in the helium flow rate on the root side of the weld did not have a significant impact on the width of the fusion zone during the welding time of 7 s.

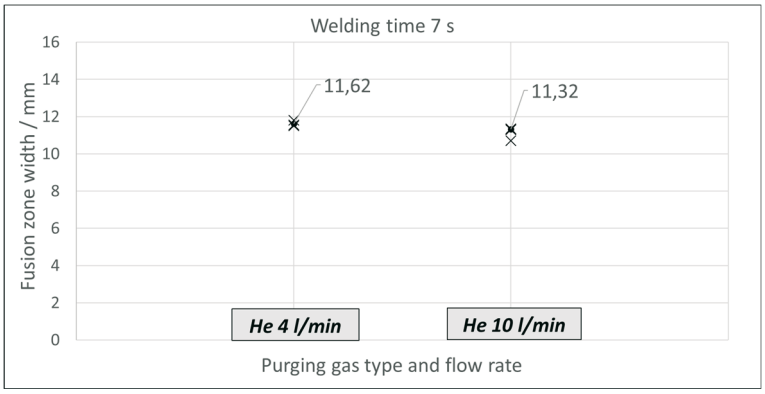


**Fig. 7** Fusion zone widths for two different helium flow rates on the weld root side

The measured depths of the fusion zones formed at helium flow rates of 4 and 10 l/min on the weld root side during a welding time of 7 s are shown in Fig. 8. The repeatability of the stationary TIG process concerning the depth of the fusion zone at a helium flow rate of 4 l/min was very good, given that the standard deviation of measured values was 0.03. However, at a helium flow rate of 10 l/min, one experiment, out of four conducted ones, resulted in a significantly greater penetration (2.58 mm) compared to the others. This can be seen in the diagram shown in Fig. 8. The recorded phenomenon impaired the reproducibility of the process. This could be the result of a change in the direction of convection in the liquid metal due to a local deviation in the content of surface-active elements (S, O, and Se) in the 316L steel. Due to the large deviation from the other values, this value of the fusion zone depth was excluded from the calculation of the mean value. Therefore, the penetration for a helium flow rate of 10 l/min has a similar value to that for a helium flow rate of 4 l/min. It follows from the above that the change in the helium flow rate on the weld root side did not significantly affect the depth of penetration.

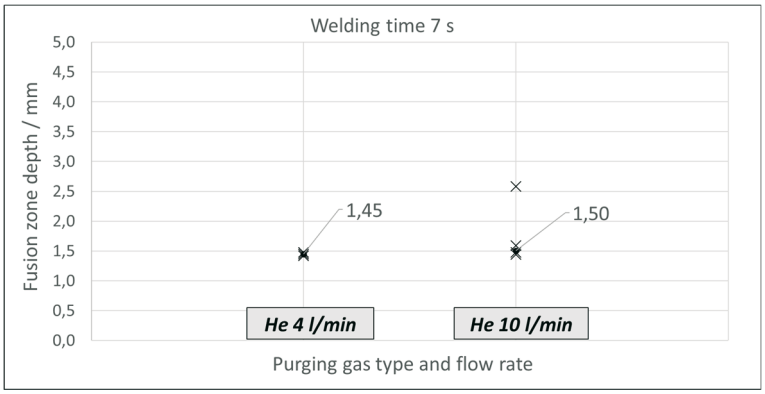


**Fig. 8** Fusion zone depths for two different helium flow rates on the weld root side

The fusion zone D/W ratios for two different helium flow rates on the weld root side and a stationary TIG welding time of 7 s are shown in Fig. 9. It is evident that the mean value of the fusion zone D/W ratio did not significantly change with an increase in the helium flow rate. One experiment conducted at a helium purging flow rate of 10 l/min was excluded from the mean value calculation because its result deviated significantly from the others.

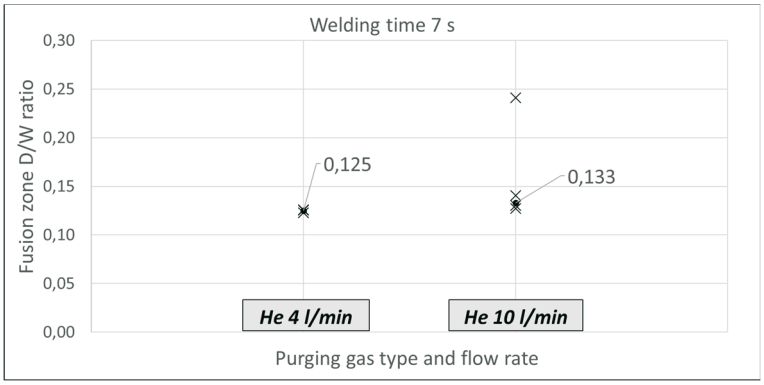


**Fig. 9** Fusion zone D/W ratio for two different helium flow rates on the weld root side

Figure 10 shows the measured values of fusion zone cross-section areas and the corresponding mean values for two different helium flow rates on the weld root side, with a welding time of 7 s. The results also indicate that increasing the helium flow rate from 4 l/min to 10 l/min did not significantly affect the average fusion zone area. The increase in the surface area was 4.2%. The experiment with results that significantly deviated from the others was also excluded from the mean value calculation.

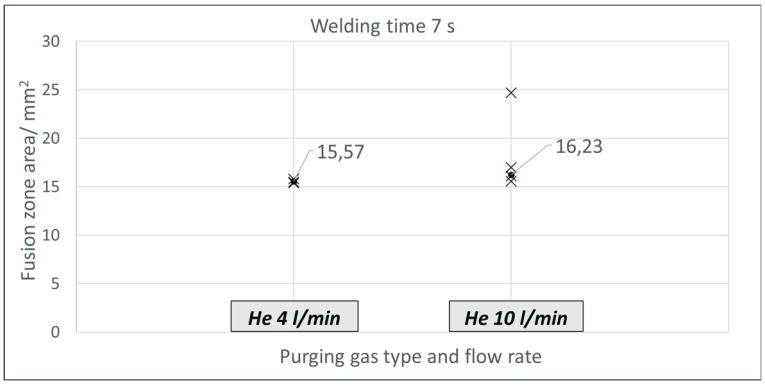


**Fig. 10** Fusion zone areas for two different helium flow rates on the weld root side

No influence of the helium purging flow rate on the fusion zone dimensions was recorded for the stationary TIG welding of 7 s. One of the specimens that showed significantly greater penetration compared to the others was excluded from the analysis.

### 4.3 Welding time 14 s; argon purging

The measured values of the fusion zone width for two different argon flows on the root side of the weld and a welding time of 14 s are shown in Fig. 11. Measurements at an argon flow rate of 4 l/min had a standard deviation of 0.48, and at a flow rate of 10 l/min the standard deviation was 0.17. This proves the good reproducibility of the stationary TIG process, considering the width of the fusion zone. This was also the case for a welding time of 7 s. The presented results indicate that there is no significant difference between the average width of the fusion zone when changing the argon flow from 4 to 10 l/min with a welding time of 14 s. The change in the average width of the fusion zone was less than 0.3%.

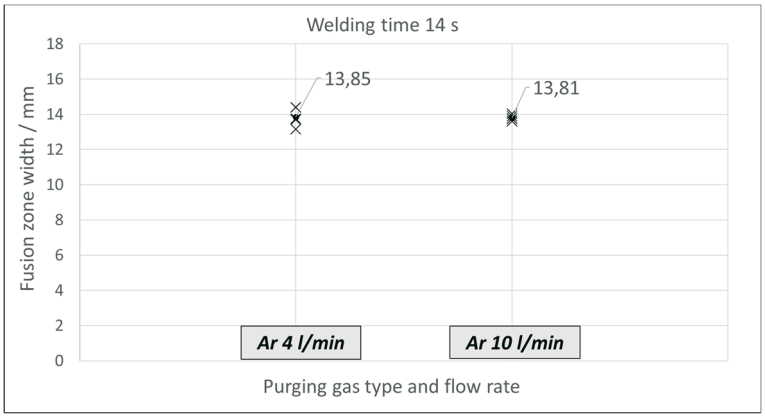


**Fig. 11** Fusion zone widths for two different argon flow rates on the weld root side

Fig. **12** shows the measured depths of the fusion zone and the corresponding mean values during a stationary TIG welding time of 14 s with two different argon flows on the root side of the weld. The measured depths of the fusion zone for the experimental categories had a standard deviation of 1.04 (Ar 4 l/min) and 0.41 (Ar 10 l/min). The repeatability of the process concerning the depth of the fusion zone is significantly worse compared to that of the welding time of 7 s. This is somewhat expected considering the larger amount of melt and the strengthening of the convective heat transfer component in the liquid metal described by the Pe number:

$$Pe = \frac{u\rho LC_p}{k} \tag{1}$$

where $u$ is the fluid flow velocity, $\rho$ is the density, $L$ is the weld pool radius, $C_p$ is the fluid heat capacity, and $k$ is the thermal conductivity.

It is known that small amounts (ppm) of surface-active elements, whose proportion in the base metal can vary locally, have a strong effect on the convection of liquid metal. Increasing the argon flow rate from 4 to 10 l/min resulted in a decrease of 3.2% in the average penetration depth. A possible reason for that may be a more intense heat removal from the root side of the specimen at a higher argon flow rate, but this value cannot be considered significant.

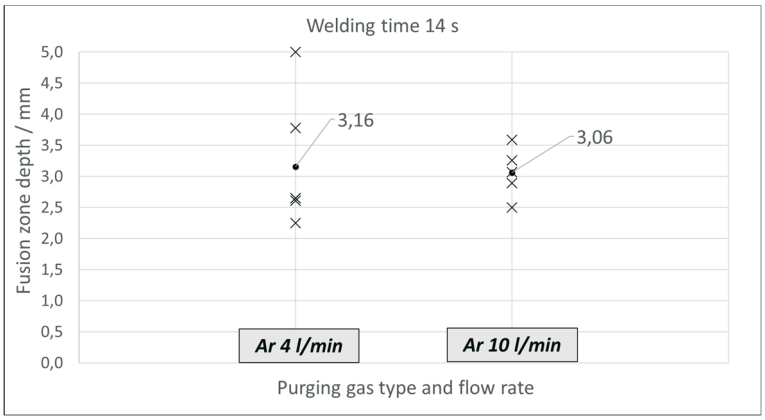


**Fig. 12** Fusion zone depths for two different argon flow rates on the weld root side

The fusion zone D/W ratios for a welding time of 14 s, with argon flow rates of 4 and 10 l/min on the weld root side, are shown in Fig. 13. The D/W ratio is determined by fusion zone depth in the first place because fusion zone widths were similar in all experiments. Thus, the fusion zone D/W ratio for an argon purging flow rate of 4 l/min is only 3.5 % higher compared to the experiments conducted at an argon purging flow rate of 10 l/min.

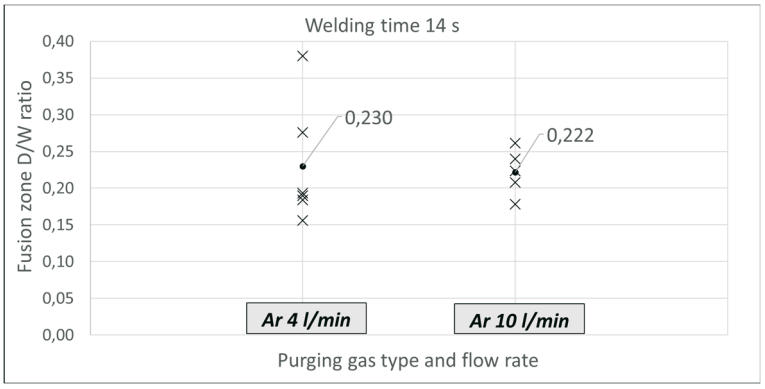


**Fig. 13** Fusion zone D/W ratios for two different argon flow rates on the weld root side

Fig. **14** shows the cross-section areas of the fusion zones and their mean values for two different argon flow rates on the weld root side of the stationary TIG process with a welding time of 14 s. The results indicate that increasing the argon purging flow rate from 4 to 10 l/min did not significantly affect the fusion zone cross-section area. The difference between the mean values was only 2.4%.

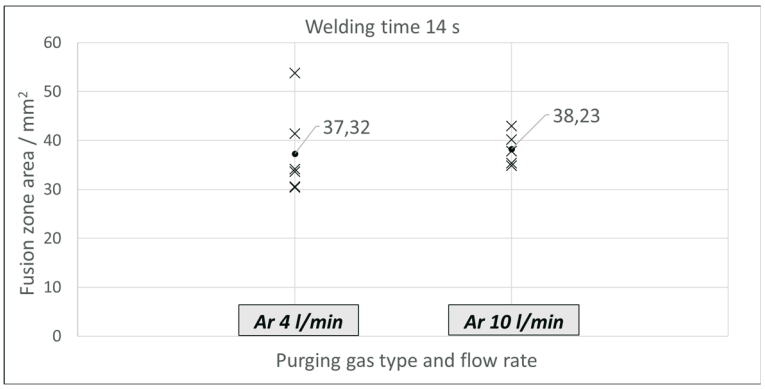


**Fig. 14** Fusion zone areas for two different argon flow rates on the weld root side

It can be stated that no strong influence of the change in the argon purging flow rate on the dimensions of the fusion zone was recorded for the stationary TIG process and welding time of 14 s.

## 4.4 Welding time: 14 s; helium purging

Fig. **15** shows the fusion zone widths and their mean values during the welding time of 14 s, with helium flow rates of 4 and 10 l/min on the root side of the weld. The repeatability of the TIG process concerning the fusion zone width remained very good compared with that for the welding time of 7 s. The standard deviation of the measured values was 0.23 (helium flow rate of 4 l/min) and 0.37 (helium flow rate of 10 l/min). The small difference between the mean values of the fusion zone width (1.8%) points to the conclusion that the change in the helium flow rate on the root side of the weld did not have a significant impact on the fusion zone width during the welding time of 14 s. The described relationship between the fusion zone width and the helium flow rate is consistent with the observations for the welding time of 7 s.

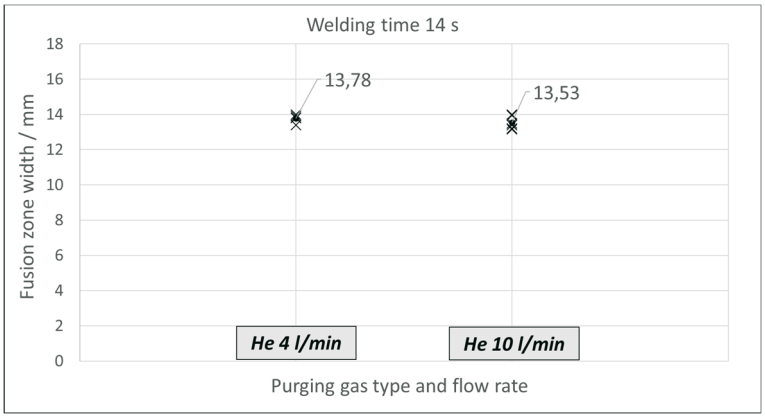


**Fig. 15** Fusion zone widths for two different helium flow rates on the weld root side

Fig. **16** shows the measured depths of the fusion zone for two different helium flow rates (4 and 10 l/min) on the root side of the weld and a welding time of 14 s. The standard deviation of the measured penetration depth at a helium flow rate of 4 l/min was 0.24. At a helium flow rate of 10 l/min, the standard deviation was 0.89, which is significantly higher than that at a helium flow rate of 4 l/min. This phenomenon could be a result of a local deviation in the content of surface-active elements (S, O, and Se) in the base metal. The mean penetration depth increased by 20.1% with the increase in the helium flow rate to 10 l/min on the root side of the weld . The results indicate that increasing the helium flow rate from 4 to 10 l/min reduces the intensity of heat removal from the root side of the weld and thus increases the penetration depth. A probable explanation is that the increased flow rate of helium (10 l/min compared to 4 l/min) reduces its average temperature on the root side of the specimen; consequently, it exhibits better insulating properties. Namely, by reducing the temperature of helium, the coefficient of thermal conductivity is also decreased.

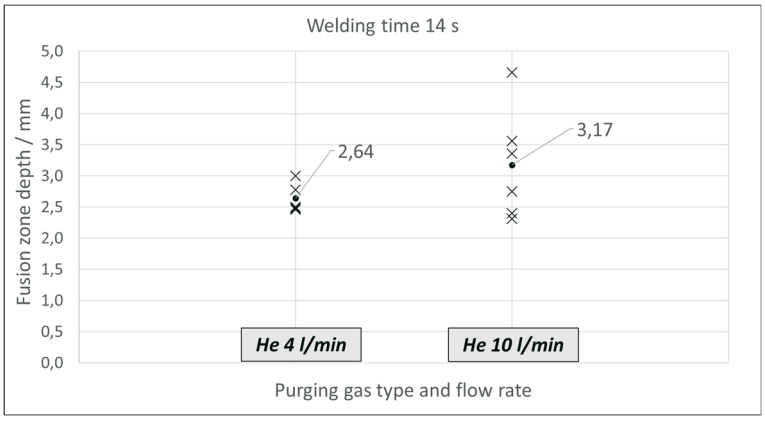


**Fig. 16** Fusion zone depths for two different helium flow rates on the weld root side

Fig. **17** shows the characteristic fusion zone D/W ratios calculated for a welding time of 14 s with two different helium flow rates on the weld root side. The D/W ratios for the two cases were determined by the fusion zone depths because the fusion zone widths were approximately equal. The presented results show that the average fusion zone D/W ratio increased by as much as 22.9% when the helium purging flow rate increased from 4 l/min to 10 l/min.

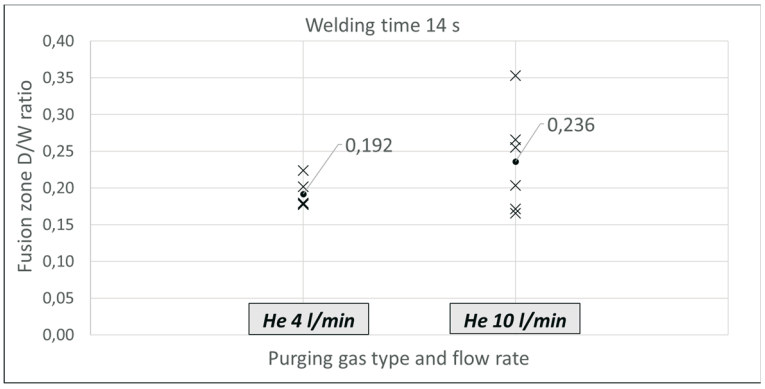


**Fig. 17** Fusion zone D/W ratios for two different helium flow rates on the weld root side

Fig. **18** showsthe measured values of the fusion zone cross-section areas and the corresponding mean values for different helium flow rates (4 l/min and 10 l/min) on the weld root side for a stationary TIG welding time of 14 s. The results indicate that there was an increase in the average fusion zone cross-section area of 10.3% when the helium flow rate was increased from 4 to 10 l/min.

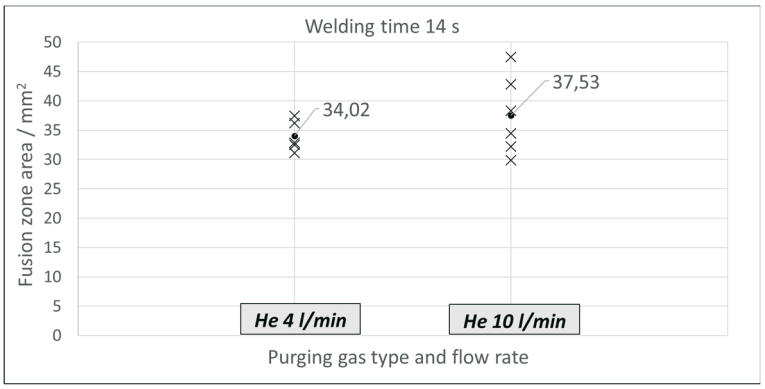


**Fig. 18** Fusion zone areas for different helium flow rates on the weld root side

During the stationary TIG welding of 14 s, an increase in the penetration depth was recorded when the helium purging flow rate was increased. A probable explanation is a decrease in the average helium temperature at a higher flow rate. This reduces the thermal conductivity coefficient of helium and thus increases the thermal insulation on the weld root side, which in turn increases the penetration depth.

### 4.5 Welding time 21 s; argon purging

The measured values of the fusion zone width for argon flow rates of 4 and 10 l/min on the root side of the weld formed during a welding time of 21 s are shown in Fig. 19. The standard deviations of measurements at argon flow rates of 4 l/min and 10 l/min were 0.59 and 0.30, respectively. Such good reproducibility of the fusion zone width was also identified with shorter welding times of 7 and 14 s. The mean values of the fusion zone width do not differ significantly (4.5%) for argon flow rates of 4 l/min or 10 l/min. This leads to the conclusion that the analysed change in the flow rate onthe weld root side did not significantly affect the fusion zone width during the welding time of 21 s.

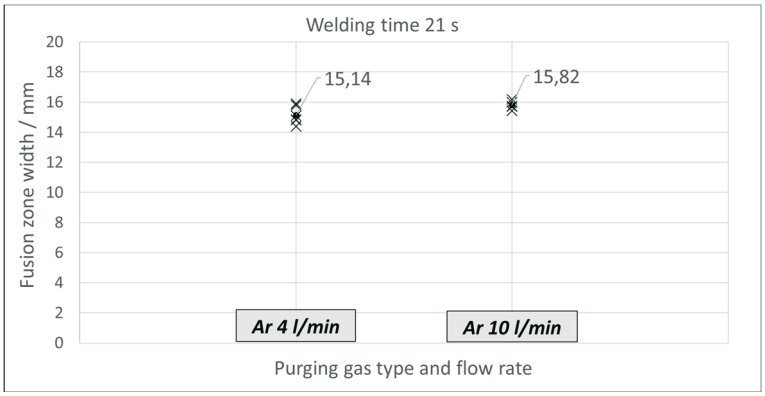


**Fig. 19** Fusion zone widths for two different argon flow rates on the weld root side

Fig. **20** shows the measured depths of the fusion zone for argon flows of 4 and 10 l/min on the weld root side. The welding time was 21 s. In the case of specimens with complete penetration, the adopted depth of the fusion zone corresponds to the thickness of the specimens (5 mm), and the width of the fusion zone on the root side has a value greater than zero. Complete penetration was achieved in 4 out of 6 specimens with lower argon flow rates (4 l/min) on the weld root side. In five experiments conducted with an argon flow rate of 10 l/min, the root side of the weld was never completely penetrated, and its average depth was 3.79 mm. This value is 17.4% lower than the depth of the fusion zones formed at an argon flow rate of 4 l/min. It can be concluded that the increase in the argon flow rate on the weld root side decreased the depth of the fusion zone during the welding time of 21 s. The same trend, but with much smaller differences in the average depth of the fusion zones, was recorded during the welding time of 14 s. This trend can propably be explained by a more intensive heat removal on the weld root side of the specimen at an argon flow rate of 10 l/min compared to that recorded at an argon flow of 4 l/min, which resulted in a shallower average penetration.

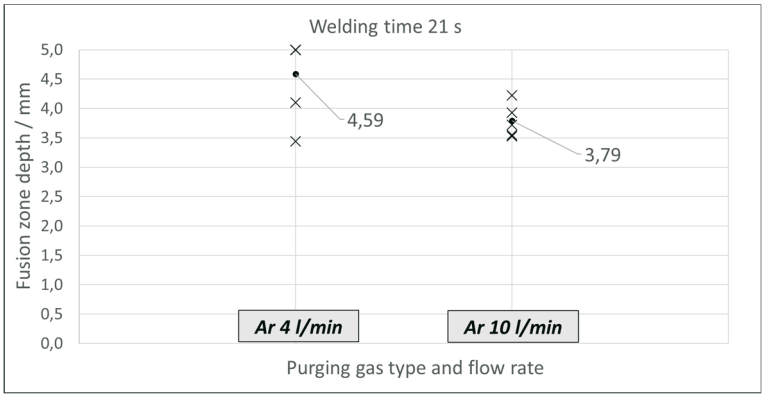


**Fig. 20** Fusion zone depths for two different argon flow rates on the weld root side

The fusion zone D/W ratios for a stationary TIG welding time of 21 s and argon flow rates of 4 and 10 l/min on the weld root side are shown in Fig. 21. A 27.1% higher average D/W ratio was achieved for the specimens with a lower argon flow rate (4 l/min). This is a direct consequence of the deeper penetration at a lower argon purging flow rate since the fusion zone widths were almost equal.

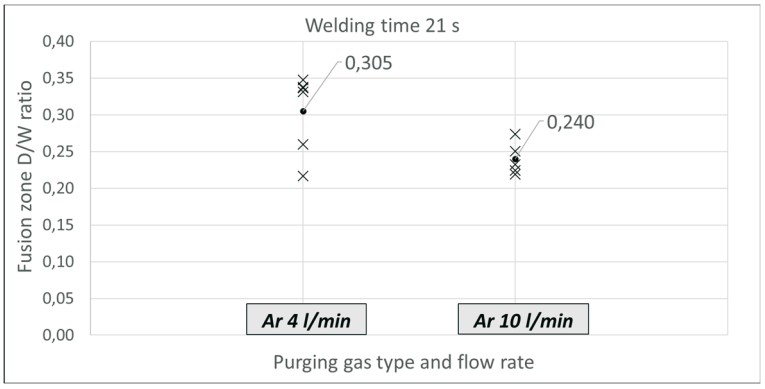


**Fig. 21** Fusion zone D/W ratios for two different argon flow rates on the weld root side

Fig. **22** shows the measured fusion zone cross-section areas and the corresponding mean values for two different argon flows (4 l/min and 10 l/min) on the weld root side and a stationary TIG welding time of 21 s. The results indicate a 24.3% decrease in the average fusion zone cross-section area when the argon purging flow rate increased from 4 to 10 l/min.

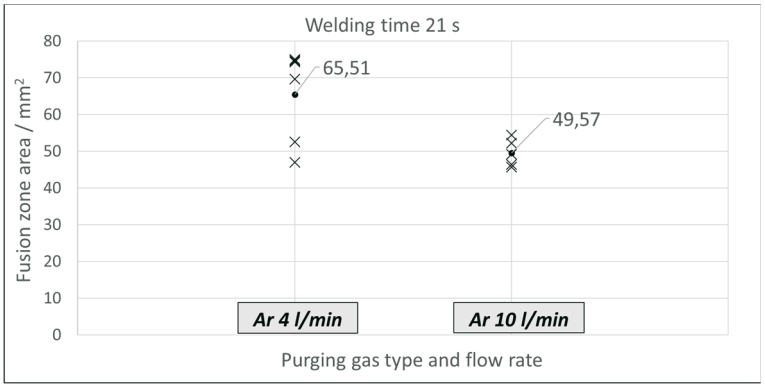


**Fig. 22** Fusion zone areas for two different argon flow rates on the weld root side

During a stationary TIG welding time of 21 s, a decrease in the penetration depth was recorded when the argon purging flow rate increased. A probable explanation is that the convective heat transfer (cooling) on the weld root side increased when the argon flow rate increased, which resulted in a shallower average penetration. This observation is in contradiction with the increase in helium purging flow rate, which resulted in a decrease in the average penetration under the same welding conditions (parameters).

### 4.6 Welding time 21 s; helium purging

Fig. **23** shows the widths of the fusion zones and their mean values for a welding time of 21 s and helium flow rates of 4 l/min and 10 l/min on the root side of the weld. The standard deviations of the measured values were 0.32 and 0.33 for helium purging flow rates of 4 l/min and 10 l/min, respectively. Based on this, it can be said that the reproducibility of the stationary TIG process concerning the width of the fusion zone remained relatively good, which was true for welding times of 7 and 14 s. The difference between the mean values of the fusion zone width of approximately 3% leads to the conclusion that the change in the helium flow rate on the root side of the weld had no significant influence on the width of the fusion zone during the welding time of 21 s. The same conclusion was also reached for shorter welding times.

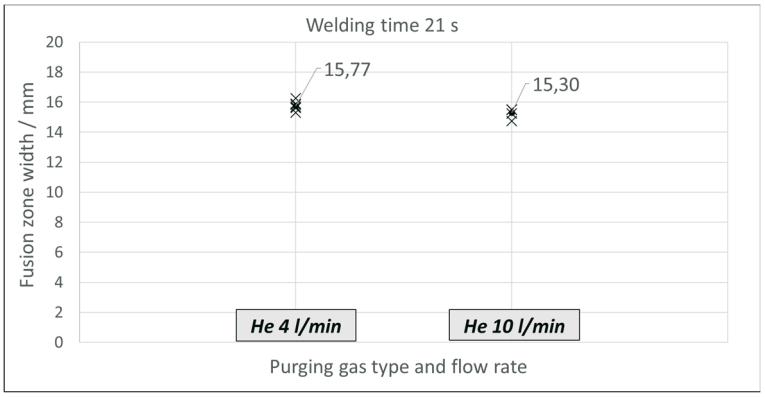


**Fig. 23** Fusion zone widths for two different helium flow rates on the weld root side

Fig. **24** shows the measured depths of the fusion zone for two different helium flow rates on the root side of the weld and a welding time of 21 s. For specimens with complete penetration, the value of the fusion zone depth, which corresponded to the thickness of the specimens (5 mm), was adopted. It can be seen that complete penetration was achieved in one experiment with a lower helium flow rate (4 l/min) on the weld root side, and the average penetration at the same helium flow rate was 3.66 mm. In experiments conducted with a helium flow rate of 10 l/min on the weld root side, the average depth of the fusion zone was 16.9% higher (4.28 mm), and complete penetration was also achieved in one of the experiments. It can be concluded that the increase in the helium flow rate on the weld root side increased the depth of the fusion zone for the welding time of 21 s. This finding is consistent with the finding for the welding time of 14 s. The possible explanation remains the same: increasing the helium flow rate from 4 to 10 l/min reduces the average temperature of helium on the weld root side and thus improves its insulating properties (reduces its thermal conductivity). Better thermal insulation of the weld root side increases the penetration depth.

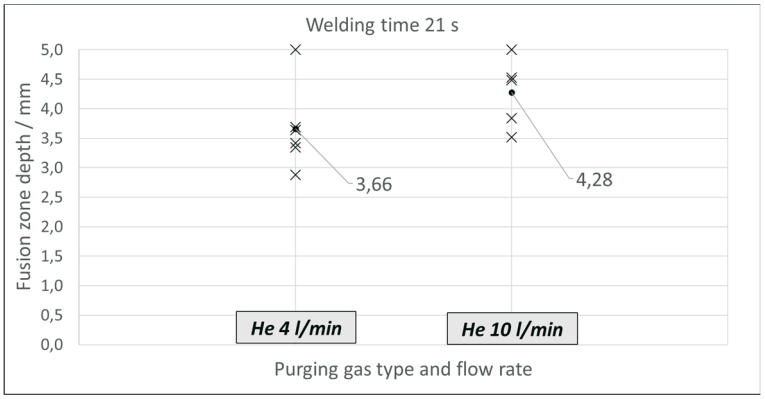


**Fig. 24** Fusion zone depths for two different helium flow rates on the weld root side

Since the conducted experiments resulted in similar fusion zone widths, the difference in the fusion zone depths was reflected in the fusion zone D/W ratio (Fig. 25). Thus, a 20% higher average fusion zone D/W ratio was achieved in the experiments conducted at a helium purging flow rate of 10 l/min compared to that achieved in the experiments at a helium purging flow rate of 4 l/min.

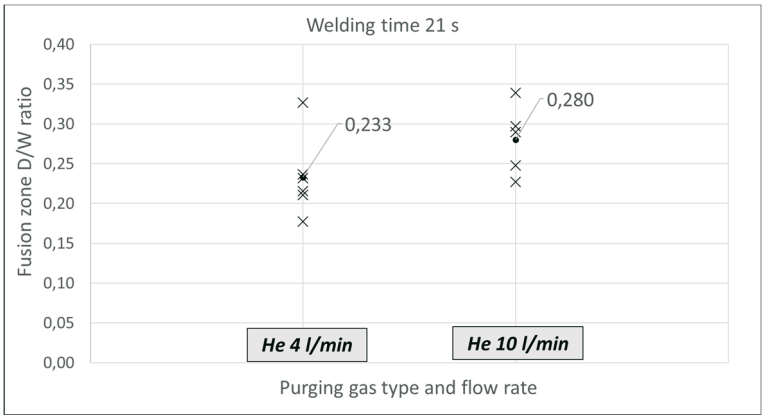


**Fig. 25** Fusion zone D/W ratios for two different helium flow rates on the weld root side

Fig. **26** shows the measured values of the fusion zone cross-section areas and the corresponding mean values for two different helium flow rates on the weld root side and a welding time of 21 s. The results show that the mean value of the fusion zone cross-section area increased by 13% when the helium purging flow rate increased from 4 l/min to 10 l/min.

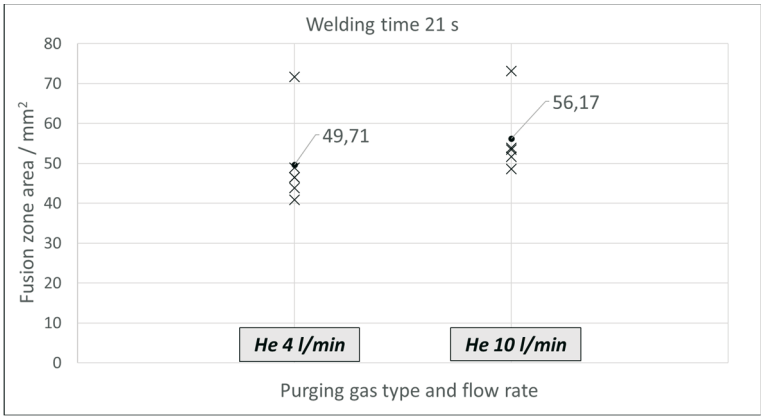


**Fig. 26** Fusion zone areas for two different helium flow rates on the weld root side

During a stationary TIG welding time of 21 s, an increase in the penetration depth was recorded when the helium purging flow rate increased from 4 l/min to 10 l/min. The same phenomenon was recorded for a welding time of 14 s. These results are in contrast with the results obtained for the increased argon purging flow rate, probably due to the significantly different physical properties of the two gases. Argon is a gas with a significantly higher density than helium, and its thermal conductivity coefficient is much lower. It should also be noted that significant temperature differences occur on the root side of the weld, which also affects the physical properties of these two gases. It is also possible that the regimes of gas flow (laminar, transitional, or turbulent) to the root side of the weld of argon and helium are not the same; this can significantly affect the heat transfer.

## 4.7 Fusion zone time evolution

The data in Table 12 as well as Fig. **27** and Fig. **28** show changes in the fusion zone width (FZW) for two different helium and argon flow rates on the weld root side. It is evident from the results that the analyzed changes in the helium and argon flow rates (4 and 10 l/min) did not significantly affect the average width of the fusion zone. The line equations that describe the time-related change in the fusion zone width are very similar. This indicates that the time-related increase in the width of the fusion zone in the 7–14 s interval had similar dynamics regardless of the gas flow on the root side of the weld.

**Table 12** Average fusion zone widths (mm) for two different argon and helium root side flow rates

| | *Welding time* (WT) | | | | | |
|---|---|---|---|---|---|---|
| *Gas and flow rate* | 7 s | 14 s | 21 s | *Equation* | | $R^2$ |
| Ar 4 l/min | 11.42 | 13.85 | 15.14 | $FZW = 0.27 \cdot WT + 9.74$ | (2) | 0.97 |
| Ar 10 l/min | 11.78 | 13.81 | 15.82 | $FZW = 0.29 \cdot WT + 9.77$ | (3) | 1.00 |
| He 4 l/min | 11.62 | 13.78 | 15.77 | $FZW = 0.30 \cdot WT + 9.57$ | (4) | 0.99 |
| He 10 l/min | 11.32 | 13.53 | 15.30 | $FZW = 0.28 \cdot WT + 9.40$ | (5) | 0.99 |

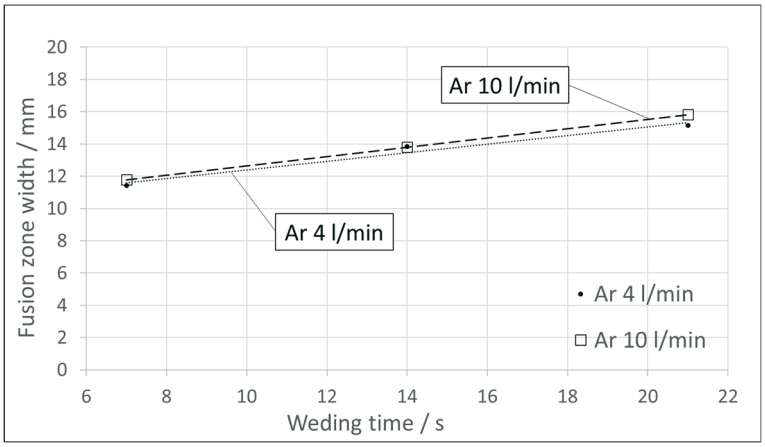


**Fig. 27** Fusion zone width evolution, weld root side argon-shielded

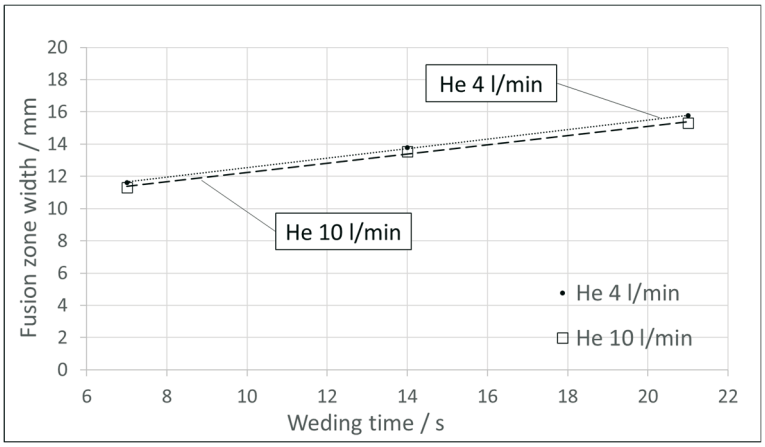


**Fig. 28** Fusion zone width evolution, weld root side helium-shielded

The calculated average fusion zone depths (FZD) for the protection of the weld root side with argon and helium are shown in Table 13. The results are graphically shown in Fig. 29 and Fig. **30**. The line equations that describe the time-related change in the fusion zone depth in the observed interval (7–14 s) indicate that the penetration depth increased faster when the root side was shielded using an argon flow rate of 4 l/min (0.22 mm/s) than in the case with an argon flow rate of 10 l/min (0.17 mm/s). When the root side was shielded using helium, the trend was the opposite: the average penetration increased faster when a helium flow rate of 10 l/min (0.20 mm/s) was used than in the case with a helium flow of 4 l/min (0.16 mm/s). The difference in the dynamics of penetration increase between argon and helium is a consequence of the fundamentally different physical properties of the two gases, which affect the intensity of heat transfer on the root side of the weld.

**Table 13** Average fusion zone depths (mm) for two different argon and helium root side flow rates

| | *Welding time* | | | | | |
|---|---|---|---|---|---|---|
| *Gas and flow rate* | 7s | 14 s | 21 s | *Equation* | | $R^2$ |
| Ar 4 l/min | 1.56 | 3.16 | 4.59 | $\mathrm{FZD} = 0.22 \cdot WT + 0.08$ | (6) | 0.99 |
| Ar 10 l/min | 1.46 | 3.06 | 3.79 | $\mathrm{FZD} = -0.01 \cdot WT^2 + 0.42 \cdot \mathrm{WT} - 1.01$ | (7) | 1.00 |
| He 4 l/min | 1.45 | 2.64 | 3.66 | $\mathrm{FZD} = 0.16 \cdot WT + 0.37$ | (8) | 0.99 |
| He 10 l/min | 1.50 | 3.17 | 4.28 | $\mathrm{FZD} = 0.20 \cdot \mathrm{WT} + 0.21$ | (9) | 0.98 |

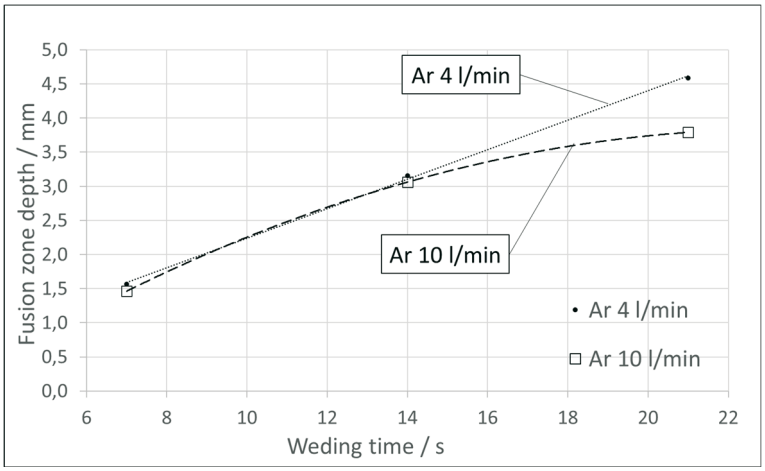


**Fig. 29** Fusion zone depth evolution, weld root side argon-shielded

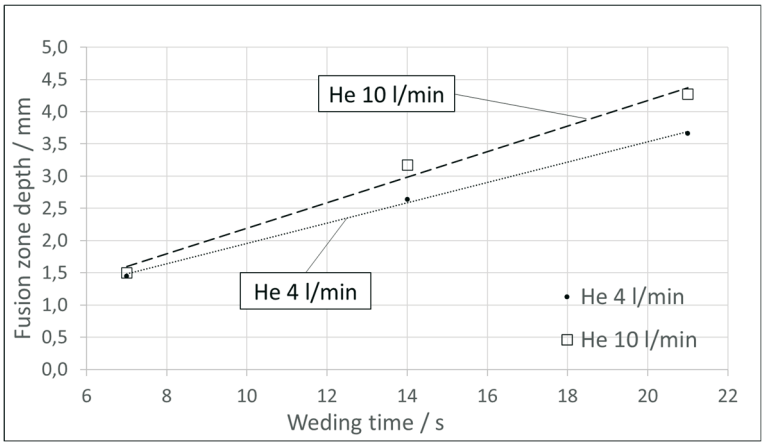


**Fig. 30** Fusion zone depth evolution, weld root side helium-shielded

The mean values of the fusion zone cross-section area (FZA) for two different flow rates of helium and argon on the weld root side and three different welding times (WT) are listed in Table 14. The results are also shown graphically in Fig. 31 and Fig**. 32**. In the case of a change in the argon flow rate on the root side of the weld, faster growth of the fusion zone area can be observed at a flow rate of 4 l/min (3.71 $mm^2/s$) compared to that at a flow rate of 10 l/min (2.45 $mm^2/s$). When the root side was protected with helium, this relationship changed. The increase in the average area of the fusion zone was slightly bigger at a helium flow rate of 10 l/min (2.85 $mm^2/s$) compared to that at a flow rate of 4 l/min (2.45 $mm^2/s$).

**Table 14** Average fusion zone cross-section area ($mm^2$) for two different argon and helium flow rates on the weld root side

| | *Welding time* | | | | | |
|---|---|---|---|---|---|---|
| *Gas and flow rate* | 7s | 14 s | 21 s | *Equation* | | $R^2$ |
| Ar 4 l/min | 16.22 | 37.32 | 65.51 | $\mathrm{FZA} = 2.52 \cdot \mathrm{WT} - 9.61$ | (10) | 0.99 |
| Ar 10 l/min | 15.34 | 38.23 | 49.57 | $\mathrm{FZA} = -0.18 \cdot WT^2 + 5.74 \cdot \mathrm{WT} - 19.1$ | (11) | 1.00 |
| He 4 l/min | 15.57 | 34.02 | 49.71 | $\mathrm{FZA} = 2.44 \cdot \mathrm{WT} - 1.04$ | (12) | 0.99 |
| He 10 l/min | 16.23 | 37.53 | 56.17 | $\mathrm{FZA} = 2.85 \cdot \mathrm{WT} - 3.30$ | (13) | 0.99 |

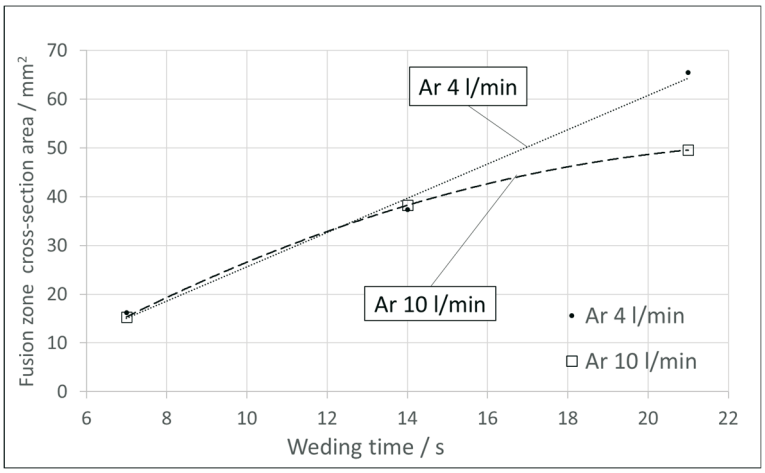


**Fig. 31** Fusion zone cross-section area evolution, weld root side argon-shielded

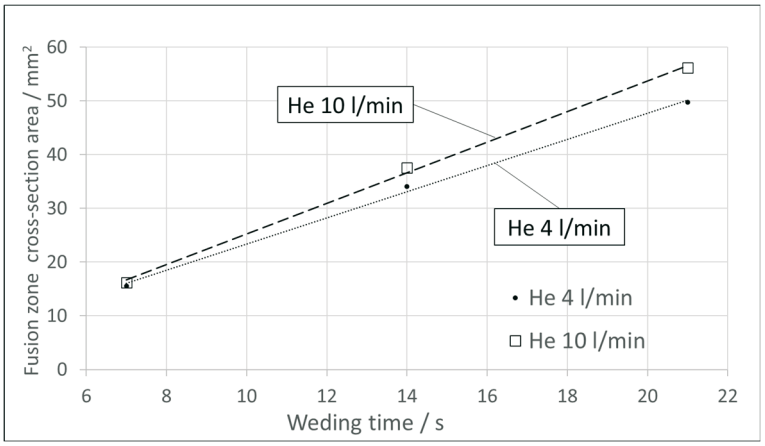


**Fig. 32** Fusion zone cross-section area evolution, weld root side helium-shielded

Tables 15 and 16 show the photos of selected fusion zone cross-sections. The shown fusion zones were formed attwo different argon or helium weld root purging flow rates (4 or 10 l/min) and three stationary TIG welding times (7, 14, or 21 s). The fusion zone cross-section photos show the differences in the weld penetration profile caused by the two different purging gas flow rates and three welding times.

**Table 15** Fusion zone cross-sections for two different argon purging flow rates on the weld root side and three welding times

| | Ar 4 l/min | Ar 10 l/min |
|---|---|---|
| 7 s | 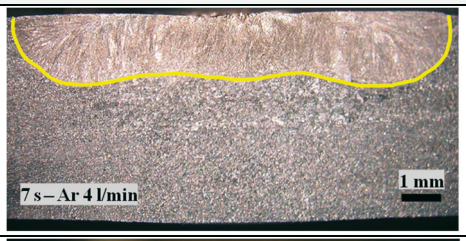  | 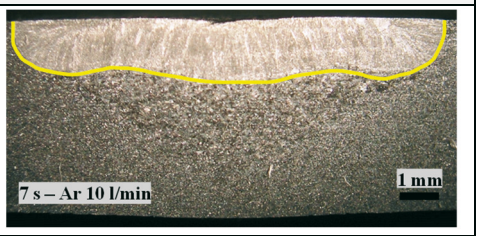  |
| 14 s | 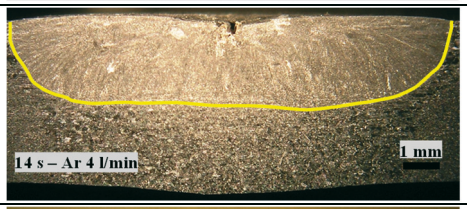  | 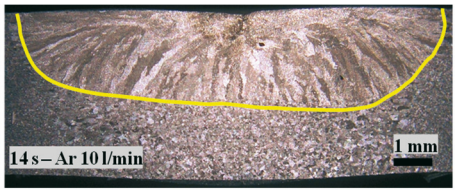  |
| 21 s | 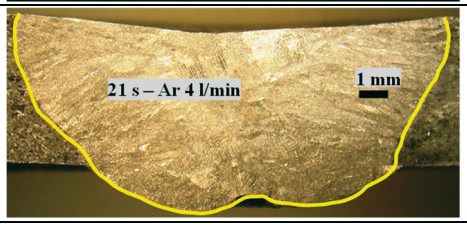  | 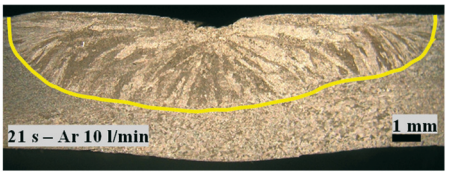  |

**Table 16** Fusion zone cross-sections for two different helium purging flow rates on the weld root side and three welding times

| | He 4 l/min | He 10 l/min |
|---|---|---|
| 7 s | 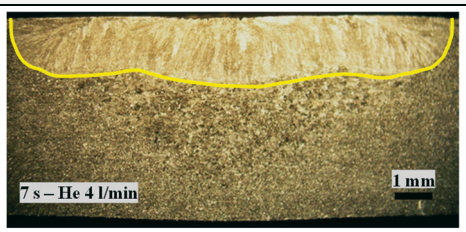  | 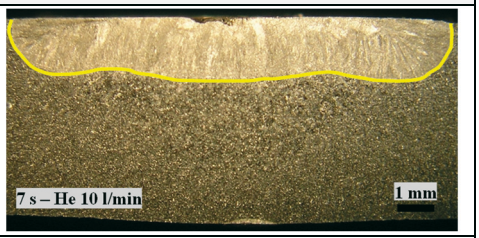  |
| 14 s | 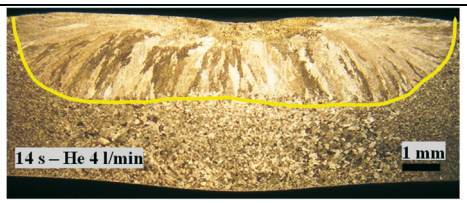  | 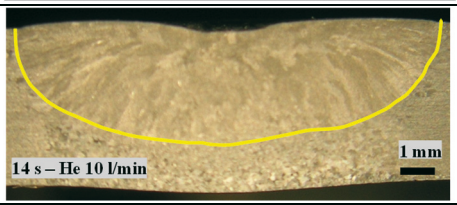  |
| 21 s |   | 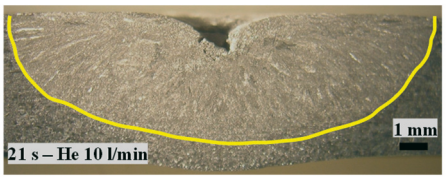  |

## 5. Conclusions

The purpose of thisstudy was to determine the influence of the argon and helium weld root side purging flow rates on the fusion zone width, depth, cross-section area, and D/W ratio. The chosen flow rates of purging gases were 4 and 10 l/min. A stationary autogenous TIG process using direct current (150 A) and welding times of 7, 14, and 21 s were used in the welding experiments. The specimens with dimensions of 100x100 mm were made from 5 mm-thick 316L austenitic stainless steel. The findings of this research provide a few new insights into the influence of the purging gas flow rate on the fusion zone dimensions:

- No significant influence of the argon and helium purging flow rates on the measured fusion zone dimensions was determined for awelding time of 7 s. The relatively short welding time was probably not long enough for the effect of the purging gas flow rate to be reflected in the fusion zone dimensions.
- The change in the argon purging flow rate from 4 l/min to 10 l/min had no significant impact on the fusion zone width and depth for a stationary TIG welding time of 14 s. However, the increase in helium purging rate resulted in a weld penetration increase of 20 % without affecting the fusion zone width.
- The increase in argon purging flow rate decreased the penetration depth by 17 % for a welding time of 21 s. The opposite effect was found for the increase in the helium purging flow rate: the penetration depth increased by 17 %. The width of the fusion zone did not depend on the purging gas flow rate.

Overall, the findings from this study suggest using argon weld root purging with as low a flow rate as possible. This should increase the penetration depth and reduce production costs. The fundamentally different effects of the helium and argon flow rates on the fusion zone are probably due to the radically different physical properties of the two gases. Higher purging gas flow rate can reduce the penetration depth if it intensifies the cooling of the weld root side. On the other hand, an increased flow rate reduces the average purging gas temperature, which improves the insulating characteristics of the gas due to a lower thermal conductivity coefficient at lower temperatures. Additional information on argon and helium weld root purging heat transfer dynamics requires further investigation.

## REFERENCES

[1] J. C. Lippold, D. J. Kotecki, *Welding Metallurgy and Weldability of Stainless Steel*, John Wiley & Sons, Hoboken, 2005.

[2] E. Folkhard, *Welding Metallurgy of Stainless Steels*, Springer Vienna, Vienna, 1988. https://doi.org/10.1007/978-3-7091-8965-8

[3] American Welding Society, *Welding Handbook: Welding Processes, Part 1*, American Welding Society, Miami, 2004.

[4] M. Mariappan, N. Parthasarathi, R. Ravindran, K. Lenin, A. Palanisamy, Improvement of Weld Bead Characteristics in Gas Metal Arc Welding of SA515 Carbon Steel by Applying Alternating Shielding Gas Flow Technique, *Transactions of FAMENA*, 2023, 47, 67–85. https://doi.org/10.21278/TOF.471032821

[5] E. Bajramović, D. Gačo, F. Islamović, Behaviour of High-Alloy Steel Welded Joints of Steam Pipelines under the Influence of Temperature and Exploitation Time, *Transactions of FAMENA*, 2022, 46, 103–113. https://doi.org/10.21278/TOF.463039822

[6] K. Karthick, G. Magudeeeswaran, Effects of Gas Metal Arc Welding Variants on the Mechanical and Microstructural Characteristics of AISI 304 Stainless Steel, *Transactions of FAMENA*, 2023, 47, 31–46. https://doi.org/10.21278/TOF.473048822

[7] T. DebRoy, S. A. David, Physical processes in fusion welding, *Reviews of Modern Physics*, 1995, 67, 85–112, 10.1103/RevModPhys.67.85. https://doi.org/10.1103/RevModPhys.67.85

[8] F. Wu, K. V. Falch, D. Guo, P. English, M. Drakopoulos, W. Mirihanage, Time evolved force domination in arc weld pools, *Materials & Design*, 2020, 190, 1–8. https://doi.org/10.1016/j.matdes.2020.108534

[9] L. Aucott, H. Dong, W. Mirihanage, R. Atwood, A. et al. Kidess, Revealing internal flow behaviour in arc welding and additive manufacturing of metals, *Nature Communications*, 2018, 9, 1–7. https://doi.org/10.1038/s41467-018-07900-9

[10] S. P. Lu, H. Fujii, K. Nogi, T. Sato, Effect of oxygen content in He-O2 shielding gas on weld shape in ultra deep penetration TIG, *Science and Technology of Welding and Joining*, 2007, 12, 689–695. https://doi.org/10.1179/174329307X238425

[11] H. Jamshidi Aval, A. Farzadi, S. Serajzadeh, A. H. Kokabi, Theoretical and experimental study of microstructures and weld pool geometry during GTAW of 304 stainless steel, *International Journal of Advanced Manufacturing Technology*, 2009, 42, 1043–1051. https://doi.org/10.1007/s00170-008-1663-6

[12] A. Shirali, K. Mills, The effect of welding parameters on penetration in GTA welds, *Welding journal*, 1993, 72, 347–353,

[13] H. Y. Huang, Effects of shielding gas composition and activating flux on GTAW weldments, *Materials and Design*, 2009, 30, 2404–2409. https://doi.org/10.1016/j.matdes.2008.10.024

[14] H. Huang, S. Shyu, K. Tseng, C. Chou, Efects of the Process Parameters on Austenitic Stainless Steel by TIG-Flux Welding, *Journal of Materials Science & Technology*, 2006, 22, 367–374,

[15] C. R. Heiple, J. R. Roper, Mechanism for Minor Element Effect on GTA Fusion Zone Geometry, *Welding Journal*, 1982, 61, 97–102,

[16] P. Burgardt, C. R. Heiple, Interaction between Impurities and Welding Variables in Determining GTA Weld Shape, *Welding Journal*, 1986, 2, 150–155,

[17] V. A. Karkhin, *Thermal processes in welding*, Springer Nature Singapore, Singapore, 2019. https://doi.org/10.1007/978-981-13-5965-1

[18] E. Taban, E. Kaluc, T. S. Aykan, Effect of the purging gas on properties of 304H GTA welds, *Welding Journal*, 2014, 93.

[19] E. M. Westin, M. M. Johansson, R. F. A. Pettersson, Effect of nitrogen-containing shielding and backing gas on the pitting corrosion resistance of welded lean duplex stainless steel LDX 2101® (EN 1.4162, UNS S32101), *Welding in the World*, 2013, 57, 467–476. https://doi.org/10.1007/s40194-013-0046-2

[20] P. Panmongkol, I. Phung-on, Effect of backing gas mixtures on corrosion properties of stainless steel grade 304 weld metal by autogenous GTAW, *Journal of Materials Research and Technology*, 2021, 11, 1559–1570. https://doi.org/10.1016/j.jmrt.2021.01.125

[21] E. L. Bergquist, T. Huhtala, L. Karlsson, The effect of purging gas on 308L tig root-pass ferrite content, *Welding in the World*, 2011, 55, 57–64. https://doi.org/10.1007/BF03321287

[22] M. Stadler, P. Freton, J. J. Gonzalez, Influence of welding parameters on the weld pool dimensions and shape in a TIG configuration, *Applied Sciences*, 2017, 7, 1–16. https://doi.org/10.3390/app7040373

[23] M. Stadler, M. Masquère, P. Freton, J. J. Gonzalez, Experimental characterisation of the weld pool expansion in a tungsten inert gas configuration, *Science and Technology of Welding and Joining*, 2017, 22, 319–326. https://doi.org/10.1080/13621718.2016.1235878

[24] D. Kojundžić, N. Krnić, I. Samardžić, Influence of Purging Gas on 316L Stainless Steel Fusion Zone in Autogenous Stationary TIG Welding, *Tehnicki vjesnik - Technical Gazette*, 2022, 29, 1–10. https://doi.org/10.17559/TV-20220407215830

[25] P. Pichler, B. J. Simonds, J. W. Sowards, G. Pottlacher, Measurements of thermophysical properties of solid and liquid NIST SRM 316L stainless steel, *Journal of Materials Science*, 2020, 55, 4081–4093. https://doi.org/10.1007/s10853-019-04261-6

[26] M. I. Boulos, P. Fauchais, E. Pfender, *Thermal Plasmas - Fundamentals and Applications - Volume 1*, Springer Science+Business Media, New York, 1994. https://doi.org/10.1007/978-1-4899-1337-1_1

Submitted: 27.5.2023

Accepted: 26.7.2023

Domagoj Kojundžić, PhD Student*
Nikša Krnić, Associate Professor, PhD.
Faculty of Electrical Engineering, Mechanical Engineering and Naval Architecture, Ruđera Boškovića 32, 21000 Split, Croatia
Zoran Kožuh, Full professor tenure
Faculty of Mechanical Engineering and Naval Architecture, Ivana Lučića 5, 10000 Zagreb, Croatia
*Corresponding author:
dkojundz@fesb.hr